RSC Advances

ROYAL SOCIETY OF CHEMISTRY

www.rsc.org/advances

Cite this: DOI: 10.1039/c0xx00000x

www.rsc.org/xxxxxx

ARTICLE TYPE

The energy band tailored by Al incorporation in solution-processed IZO TFTs

Yana Gao[a], Jianguo Lu[b], Jianhua Zhang[a] and Xifeng Li*[a]

Received (in XXX, XXX) Xth XXXXXXXXX 20XX, Accepted Xth XXXXXXXXX 20XX

DOI: 10.1039/b000000x

The energy band tailoring of indium zinc oxide (IZO) through Al incorporation was studied and measured directly by ultraviolet photoelectron spectroscopy (UPS). Al doped IZO (AIZO) thin films have lower work function (3.90 eV) and wider bandgap (3.75 eV) compared with IZO (4.15 and 3.5 eV, respectively). These changes induced by Al incorporation would result in higher activation energy and higher flat voltage for AIZO TFTs, which may imply the origin of the AIZO TFTs electrical properties such as threshold voltage shift and off-state current decrease.

Introduction

Amorphous oxide semiconductors (AOSs) are promising candidates as transparent semiconductors for use in the active-matrix backplanes of next-generation displays due to their high carrier mobility, favorable environmental/thermal stability, good optical transparency in visible region, and potential for low temperature film processing [1-6]. However, thin film transistors (TFTs) fabricated with binary oxide semiconductors based on ZnO, In_2O_3 have some issues such as the instability and high off-state current [2-5]. To address the problems, numerous channel materials incorporating a third suppressor element such as ZrInZnO [2, 4], HfInZnO [6], AlInZnO [7, 8] etc. have been investigated since the first use of Ga in 2004 [1]. Among them, Al was a low cost element and also has a lower standard electrode potential (SEP) (-1.66 V) which makes it more efficiently suppress oxygen-vacancy formation and hence help to achieve a lower off-state current and a large on-to-off current ratio [9]. Moreover, Al_2O_3 has a remarkably larger bandgap (Eg) of ~ 9 eV [10], compared to other similar oxide such as ZnO (3.3 eV) and In_2O_3 (3.6 eV) [3]. Therefore, it can be expected that the incorporation of Al can control the film electrical characteristics and improve the device performance by controlling the oxygen vacancies and Eg.

Nowadays, most studies on AIZO semiconductors were focused on the fluctuation of oxygen vacancy amount and carrier concentration of those [7, 8]. However, development of emerging and future applications in the area of thin film transistors with oxide semiconductors requires a detailed control of Fermi level position and a depth study on carrier conduction mechanism [11]. In this work, work functions, energy band gap as well as energy band alignment at interfaces influencing carrier conduction are described and discussed. It provides a fundamental understanding of AIZO thin film transistors performance in terms of the energy band tailored by Al incorporation. An intuitional measurement of AIZO work function and valance band energy level was conducted by ultraviolet photoelectron spectroscopy (UPS) along with the UV-visible spectroscopy analysis. The results show that AIZO films have wider energy bandgap and lower work function compared with IZO films. In this paper, we investigated the difference of IZO and AIZO in terms of band bending and carrier conduction mechanism which can explain the reduced off-state current and positive shifted threshold voltage. In addition, chemical solution deposition processes are the most promising for direct deposition, low cost manufacturing, and various compositions of oxide thin films [2, 6]. Hence, solution processed both oxide semiconductor and gate dielectric TFTs were fabricated in our paper.

Experimental

A 0.3 M AIZO precursor was synthesized by dissolving Aluminum chloride ($AlCl_3$), zinc acetate dihydrate ($Zn(CH_3COO)_2{\cdot}2H_2O$) and indium nitrate hydrate ($In(NO_3)_3{\cdot}xH_2O$) into 2-methoxyethanol (2-MOE). Additionally 0.3 M monoethanolamine (MEA) was added for long-term solution stability. The atomic ratio of In : Zn was fixed at 3 : 2, and that of Al : In ranged from 0 to 15 at%, (i.e., atomic ratios of Al : In : Zn = 0 ~ 0.45 : 3 : 2). Considering the fact that $AlCl_3$ is highly reactive and difficult to handle in the ambient, the first step to prepare AIZO solutions was dissolving $AlCl_3$ into 2-MOE in the glovebox with N_2 atmosphere. The mixed AIZO solutions were stirred at 400 rpm and 70 °C for 3 hours to form transparent and homogeneous solutions. The solution processed films were spin coated at 3000 rpm. The AIZO films were heated on a hot plate at 150 °C for 15 min and subsequently annealed at 300 °C for 30 min to enable gradual evaporation of the residual solvent. The solution-processed AIZO TFTs with bottom-gate structure were fabricated on a glass substrate. A 100 nm thick ITO film was sputtered on glass substrate as the bottom-gate electrode. Then the Aluminum-doped zirconium oxide (AZO) gate dielectric films were deposited by spin-coating [12]. A 50 nm thick ITO film as the source and drain electrodes were fabricated also by sputtering. Eventually, the AIZO active layer was

subsequently spin-coated on the prepared substrate. The channel width (W) and length (L) ratio of the fabricated TFTs was 5 (L = 20 um). As we have reported, the relative dielectric constant extracted from a metal-insulator-metal (MIM) capacitor structure was 19.67 [12]. The Hall mobility, carrier concentration and conductivity were measured by Hall measurement system (HL5500, Bio-Rad). The optical properties were characterized using UV-visible spectrometer (H-3900, Hatachi). The surface properties and compositions of film were examined using an x-ray photoelectron spectroscopy (XPS, Thermo-VG ESCALAB 250) and an UPS. The carbon 1s peak at 284.6 eV was used as a reference for calibration in the XPS results. Grazing incidence X-ray diffraction (XRD, D/MAX-2550) was used to identify phase of the films. The TFTs electrical properties were measured in dark and air using an Agilent 4155C semiconductor parameter analyzer.

Result and Discussion

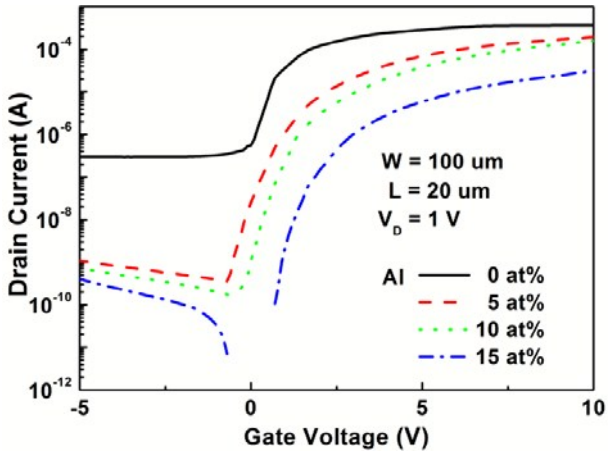

Figure 1: (Color on-line) Transfer (I_{DS}-V_{GS}) characteristics of solution processed AIZO TFTs as a function of the Al amounts from 0 to 15 at%. The AIZO TFTs were annealed at 300 °C

Table I. Extracted device parameters of AIZO TFTs annealed at 300 °C with the different mole ratio of Al.

Al (at%)	u_{sat} (cm^2/Vs)	$I_{on/off}$	V_T (V)	$S.S$ (V/dec)
0	16.99	1.4×10^3	-	-
5	8.03	5.7×10^5	0.49	0.76
10	6.03	1.0×10^6	0.89	0.73
15	1.3	3.0×10^6	1.56	0.51

Figure 1 shows transfer characteristics of solution processed AIZO TFTs annealed at 300 °C as a function of the Al contents from 0 to 15 at%. The measurements were performed by sweeping the gate-to-source voltage (V_{GS}) from −5 to 10 V, with a drain-to-source voltage (V_{DS}) of 1 V. The TFT electrical characteristics are summarized in table I. It was obvious that the off-state current decreased from 2.7×10^{-7} to 1.0×10^{-11} A and the threshold voltage (V_T) shift to a positive bias region from 0.49 to 1.56 V with the increase of the Al mole ratio. Also the on-off ratio increased from 1.4×10^3 to 3.0×10^6. When the doping content of Al was 15 at%, however, TFTs exhibited a really low on-state current of 3×10^{-5} A. It indicated the high Al concentration in the AIZO films lead to a relative low carrier concentration in AIZO films which was accompanied with low on–state and off-state current for these devices.

The saturation mobility (u_{sat}) extracted from the transfer curves were listed in Table I. It can be seen that the addition of Al reduces the saturation mobility which is coincident with the results reported in previous reports [7, 8]. Furthermore, the subthreshold swing was decreased with the increase of Al amounts indicating the decrease of the interface defects densities. This result was mainly originated from surface morphology of AIZO films. Figure 2 shown the RMS values of IZO and AIZO (10 at%) films annealed at different temperatures. The RMS values of AIZO films were lower than that of IZO films regardless of the annealing temperature. The smooth surface may be original to the amorphous phase of AIZO films [13]. XRD results indicated that the AIZO films stay in an amorphous phase at annealing temperatures range from 300 °C to 500 °C. These indicated that the incorporation of Al can attribute to a smoother surface for IZO films which could reduce the defects density and suppress the charge trapping in the interface between the channel and gate dielectric [12]. Thus, the S.S. was decreased with the increase of Al addition.

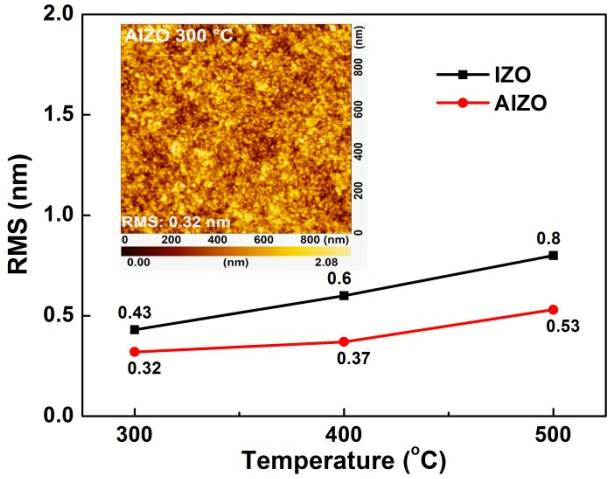

Figure 2: (Color on-line) RMS values of IZO and AIZO (10 at%) films annealed at different temperatures. Inset is the AFM image of AIZO films annealing at 300 °C

Overall TFT transfer characteristics was improved and optimized with the Al mole ratio of 10 at%. The results revealed that Al played an important role in suppressing the carrier concentration which was further confirmed by Hall measurement. Because Al atom had a relatively lower SEP than other In and Zn, it was more easily ionized and then strongly combined with oxygen atom, which reduced carrier concentration in the film due to the decrease of the oxygen vacancy serving as a source of carriers [3]. The detail effects of Al on the carrier concentration and carrier conduction were analyzed in the following sections, and we focused on the comparison between the AIZO (10 at%) and IZO solutions/films.

To further verify the effects of Al on the electrical properties IZO and AIZO films, Hall measurement was performed. Figure 3 shows the dependence of carrier concentration and resistivity on the annealing temperature of IZO and AIZO films. For AIZO films annealed at 300 °C, the Hall mobility which calculated through carrier concentration and resistivity decreased from 2.5

to 1.5 cm^2/Vs as doping of Al. The results were coincided with the changes in mobility of TFTs as shown in table I.

Moreover, the decreasing carrier concentration resulted in the increasing resistivity. Considering the results of Hall measurement, Al can suppress carrier concentration due to its low SEP (-1.66 V). The higher chemical bonding energy of Al with oxygen, rather than In or Zn, rarely provides oxygen vacancies and therefore lowers the carrier concentration [14]. Thus, Al is an effective suppressor of oxygen deficiencies generation originating from the shallow donor level in the sub gap density of states of the amorphous oxide thin film. Consequently, AIZO thin films can be used as active layer due to the decrease in shallow donor level and lowering Fermi level, which were further confirmed in the following sections. Furthermore, as the annealing temperature increased (from 300 °C to 500 °C), the carrier concentration increased and resistivity decreased. A quite similar temperature dependence of electrical behavior of other oxide semiconductors was observed [15].

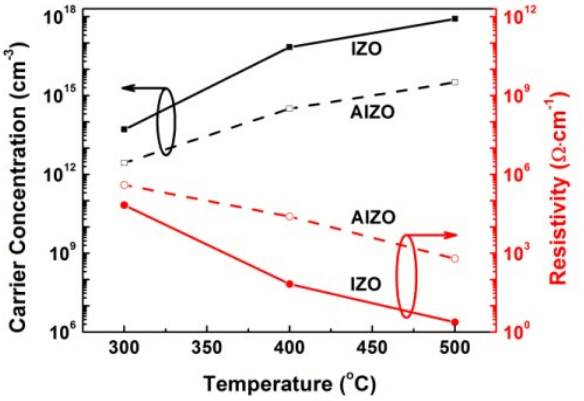

Figure 3: (Color on-line) Carrier concentration and resistivity of the IZO and AIZO films with varying temperatures (300 400 and 500 oC).

XPS measurements were performed to better understand the chemical and structural differences among AIZO and IZO films. Figure 4(a) and 4(b) shows the XPS spectra of In and Zn ions for IZO and AIZO films annealed at 300 °C. Compared the XPS spectra, it is estimated that the added Al^{3+} ions were bonded and attracted oxygen atoms connected primarily with Zn^{2+} and In^{3+} ions in the AIZO compound. As a result, the additive Al^{3+} led to the deoxidization of In-O and Zn-O bonds and a shift in the lower binding energy of Zn 2*p*3/2 and In 3*d*5/2 peaks from 1021.8 and 444.9 eV to 1021.1 and 444.5 eV [16].

Figure 4(c) and 4(d) shows oxygen 1s (O1s) XPS spectra for IZO and AIZO films annealed at 300 °C, which can be deconvoluted into three peaks, 529.9 ± 0.2 eV (peak 1), 530.8 ± 0.2 eV (peak 2), 531.7 ± 0.2 eV (peak 3), respectively. Prior studies indicate that the peak (peak 1) at 530 eV corresponds to lattice oxygen in a fully coordinated environment, while the peak (peak 2) at higher binding energies near 531 eV arise from oxygen-deficient environments, most likely to be related to oxygen vacancies [17]. And the highest binding energy peak (peak 3) is related to the oxygen in adsorbed water molecules or O-H bonding, since H is more electronegative than the metals, the M-OH oxygen atoms are less negatively charged than those in oxides, resulting in a shift toward to higher binding energy [18].

Compared the O1s XPS spectra of IZO with that of AIZO films, the relative area of peak 2 relating to the oxygen vacancy changed from 26% to 17%. This may attribute to the oxygen-aluminum ionic bonds formed in AIZO. Since the oxygen vacancy is known in general as source of the free electrons, the u_{sat} of IZO TFTs was higher than AIZO TFTs.

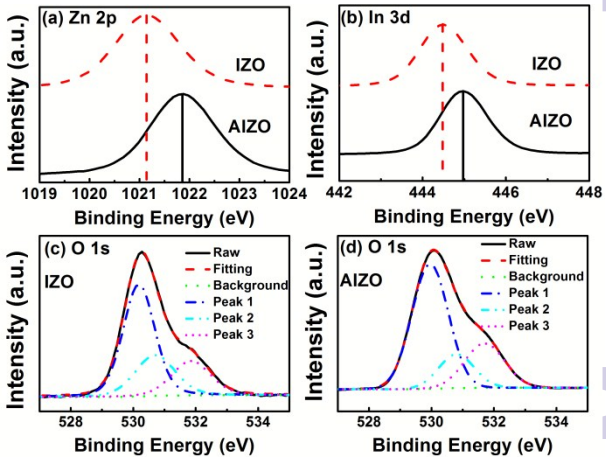

Figure 4: (color online) Zn 2p (a) and In 3d (b) spectra of IZO and AIZO films annealed at 300 °C. O1s XPS spectra of IZO (c) and AIZO (d) films annealed at 300 °C.

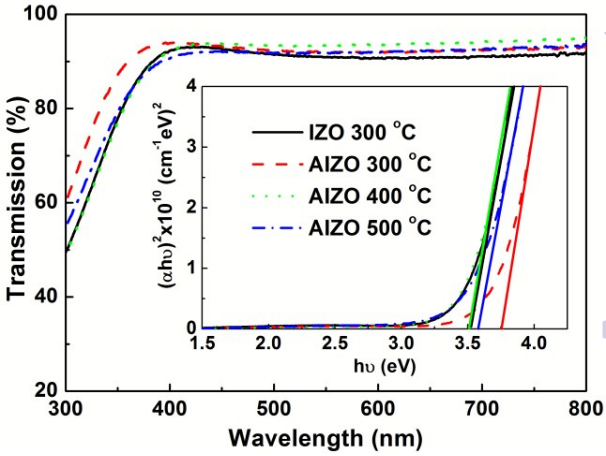

Figure 5: (Color on-line) Transmittance spectra of the intrinsic IZO films annealed at 300 oC and AIZO (Al 10 at%) films annealed at different temperatures. The inset was the (αhν)2 vs. photo energy plot of the intrinsic IZO films annealed at 300 oC and AIZO (Al: 10 at%) films annealed at different temperatures.

A suppression of carrier through incorporation of Al was observed from all above, however, the results is insufficient in explaining the mechanism of controlling the V_T and off-state current. Thus, we carried out the IZO and AIZO energy band alignment by UPS measurement. Moreover, the optical bandgap could be extracted directly by absorption coefficient as shown in figure 5.

Figure 5 shows the transmittance spectra of the IZO films and AIZO films on glass substrate through UV-visible spectroscopy. And optical bandgap of IZO and AIZO films are shown in the inset of figure 5. Compared the transmittance of films annealed at 300 °C, a blue shift in the transmittance of AIZO films from that of the IZO films was observed. The optical bandgap (*Eg*) can b

expressed by the Tuac relation [19]:

$$(\alpha hv)^2 = \mathrm{A}(hv - Eg) \quad (1)$$

where h is Planck's constant, and υ is the photon frequency, A is a constant, and Eg is the optical direct band gap, α is the absorption coefficient which obtained by equation 2 as follows:

$$\alpha = \frac{1}{d}\ln(\frac{1}{T}) \quad (2)$$

where d and T represent the film thickness and transmittance, respectively. In our experiment, the thickness of film was about 100 nm. According the transmittance of AIZO film and equation 1 and 2, the optical bandgap can be extracted. As shown in the inset of figure 5, the 300 °C annealing AIZO film has a wider bandgap of 3.75 eV than IZO film (3.5 eV). This result indicated that the addition of Al increased the bandgap, and simultaneously formed carrier suppression which was consistent with the hall measurement. Furthermore, the expansion of Eg resulted in an increase in the activation energy for donor-related shallow defect states. The fact makes the transportation of carriers to the conduction band more difficult.[3]

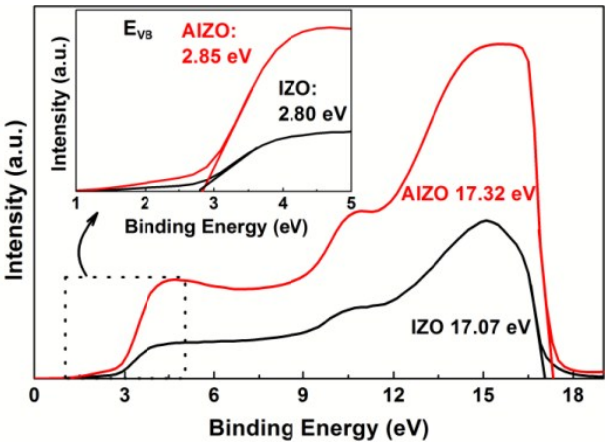

Figure 6: (Color on-line) UPS photoemission spectra of IZO and AIZO films. The inset was UPS spectra in the valence band region.

The work function and valence band energy of IZO and AIZO were measured by UPS (Figure 6). He I (21.22 eV) was utilized as a photon source for the UPS measurement. Binding energies were calibrated by measuring the Fermi step position and the Au 4*f* 7/2 core level of a clean gold film. The figure 7 shows the scale of binding energy with the Fermi level (E_F) set at 0 V. The vacuum level (E_{VAC}) should be located 21.22 eV above the cut off energy of the spectrum. According to the UPS spectrum, the value of the valence band maximum (E_{VB}) is located at 2.85 eV below the E_F for AIZO. And the work functions of IZO, AIZO based on this definition were estimated to be 4.15 and 3.90 eV, respectively. The work function of IZO was higher than AIZO, and the Fermi level of IZO was located much closer to the conduction band minimum (CBM) compared with AIZO. The distance from the CBM to the Fermi level of IZO and AIZO was 0.70 and 0.90 eV, respectively. This was in accordance with the results of Hall measurement. The higher carrier concentration of IZO induced a lower activation energy (E_C-E_F) compared to AIZO. And the bandgap of IZO was smaller than that of AIZO (Figure 5). Based on these values of IZO and AIZO films, energy-band diagrams of the AIZO and IZO films as shown in Figure 7a and 7b could be estimated.

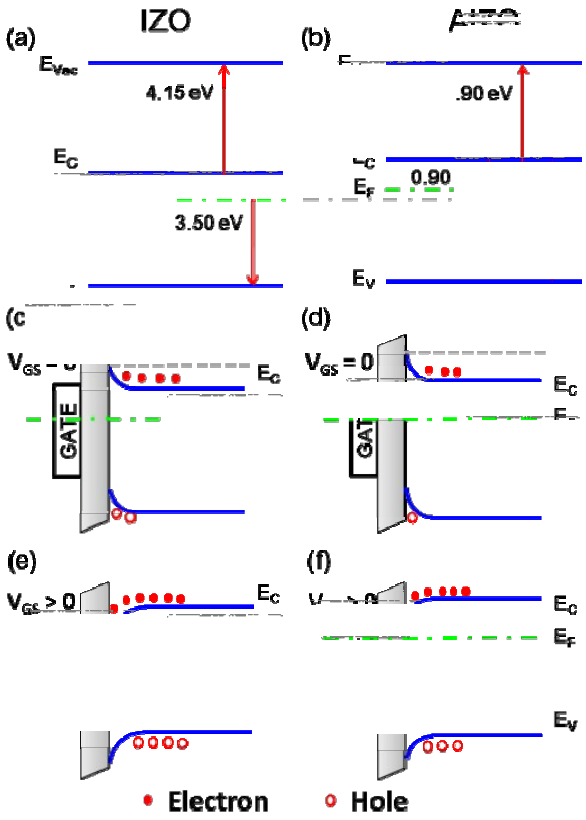

Figure 7: (Colour on-line) Energy-band diagrams of (a) IZO and (b) AIZO films. Schematic band diagram of IZO (c, e) and AIZO (d, f) TFTs under no bias stress and positive bias stress.

With regard to the work function (Φ) calculated by UPS measurement, band bending occurred between the gate and semiconductor when no gate bias stress as shown in figure 7c and 7d. The work function of ITO was 4.7 eV [20]. We ignore the influence of interface charge (Q_{int}) and the flat band voltage (V_{FB}) was determined by the work function difference between ITO and semiconductor (Φ_m-Φ_s) according to the equation 3 [21]:

$$V_{\mathrm{FB}} = \Phi_m - \Phi_s - C_{ox}^{-1}Q_{\mathrm{int}} \quad (3)$$

In general the threshold voltage is very close to the flat band voltage [22]. For AIZO TFTs, the flat voltage was larger than IZO TFTs. When gate bias increased, the separation between E_F and E_C decreased, but the separation for AIZO TFTs was larger (figure 7e and 7f). Thus, the AIZO TFTs was more difficult to operate. This may explain the positive shift of threshold voltage with different content of Al addition as shown in figure 1 and Table I. Also, the high activation energy of AIZO films would suppress the carrier generation in TFTs, and then result in a lower off-state current. All these results can verify that the addition of Al into IZO can decrease the carrier concentration and influence the carrier conduction in TFT. TFT performance can be controlled using AIZO active layer.

Conclusions

AIZO TFTs was fabricated using a solution process in this letter. Compared with IZO films, AIZO films with the Al addition had lower carrier concentration and higher resistivity. It demonstrated that Al incorporation can effectively suppress the carrier concentration due to the fact that Al is more easily ionized and strongly combined with oxygen. Furthermore, the energy band of IZO films was tailored by Al incorporation. AIZO films show a lower work function (3.90 eV) and wider bandgap (3.75 eV) resulting to higher flat band voltage and activation energy (0.90 eV). Higher flat band voltage was related to the positive shift of threshold voltage. High activation energy would suppress the carrier generation and then reduced the off-state current. The energy band alignment analysis may be beneficial for explaining the AIZO TFTs electrical properties such as the positive V_T shift and lower off-state current.

Acknowledgments

This work was supported by National Natural Science Foundation of China under Grant No 61006005, and Shanghai science and technology commission under grant No13520500200 and 14XD1401800.

Notes and references

[a] Key Laboratory of Advanced Display and System Application, Ministry of Education, Shanghai University, Shanghai 200072, China. Email:lixifeng@shu.edu.cn

[b] Key Laboratory of Silicon Materials, Department of Materials Science and Engineering, Zhejiang University, Hangzhou 310027, China

1 K. Nomura, H. Ohta, A. Takagi, T. Kamiya, M. Hirano and H. Hosono, Nature 2004, **432**, 488.
2 T. Phan Trong, T. Miyasako, L. Jinwang, T. Huynh Thi Cam, S. Inoue, E. Tokumitsu and T. Shimoda, IEEE Trans. Electron Dev. 2013, **60**, 320.
3 G. H. Kim, W. H. Jeong, B. Du Ahn, H. S. Shin, H. J. Kim, H. J. Kim, M.-K. Ryu, K.-B. Park, J.-B. Seon and S.-Y. Lee, Appl. Phys. Lett. **96**, 2010, 163506.
4 J.-S. Park, K. Kim, Y.-G. Park, Y.-G. Mo, H. D. Kim and J. K. Jeong, Adv. Mater. 2009, **21**, 329.
5 J. W. Hennek, J. Smith, A. Yan, M.-G. Kim, W. Zhao, V. P. Dravid, A. Facchetti and T. J. Marks, J. Am. Chem. Soc. 2013, **135**, 10729.
6 W. H. Jeong, G. H. Kim, H. S. Shin, B. Du Ahn, H. J. Kim, M.-K. Ryu, K.-B. Park, J.-B. Seon and S. Y. Lee, Appl. Phys. Lett. 2010, **96**, 093503 (2010).
7 Y. Lan, P. Haifeng, L. Honglei, P. Shujian and Z. Qun, J. Phys. D: Appl. Phys. 2013, **46**, 445106.
8 S. M. Park, D. H. Lee, Y. S. Lim, D. K. Kim and M. Yi, Microelectron. Eng. 2013, **109**, 189.
9 J. H. Lim, J. H. Shim, J. H. Choi, J. Joo, K. Park, H. Jeon, M. R. Moon, D. Jung, H. Kim and H.-J. Lee, Appl. Phys. Lett. 2009, **95**, 012108.
10 J. Robertson, Eur. Phys. J. Appl. Phys. 2004, **28**, 265.
11 Klein A., *J. Am. Ceram. Soc.* **96** (2013) 331.
12 Y. N. Gao, X. F. Li, L. L. Chen, J. F. Shi, X. W. Sun and J. H. Zhang, IEEE Electron Device Lett. 2014, **35**, 554.
13 Kim D. N., Kim D. L., Kim G. H., Kim S. J., Rim Y. S., Jeong W. H. and Kim H. J., *Appl. Phys. Lett.* **97** (2010) 192105.
14 K. Kyung Min, J. Woong Hee, K. Dong Lim, Y. S. Rim, Y. Choi, M. Ryu, X, Kwan, P. Kyung-Bae and K. Hyun Jae, IEEE Electron Device Lett. 2011, **32**, 1242.
15 Y. J. Kim, B. S. Yang, S. Oh, S. J. Han, H. W. Lee, J. Heo, J. K. Jeong and H. J. Kim, ACS Appl. Mater. Interfaces 2013, **5**, 3255.
16 D. N. Kim, D. L. Kim, G. H. Kim, S. J. Kim, Y. S. Rim, W. H. Jeong and H. J. Kim, Appl. Phys. Lett. 2010, **97**, 192105.
17 H.-S. Kim, J. S. Park, H.-K. Jeong, K. S. Son, T. S. Kim, J.-B. Seon, E. Lee, J. G. Chung, D. H. Kim, M. Ryu and S. Y. Lee, ACS Appl. Mater. Interfaces **4**, 2012, 5416.
18 S. Jeong, Y. G. Ha, J. Moon, A. Facchetti and T. J. Marks, Adv. Mater. 2010, **22**, 1346.
19 K.-H. Lim, K. Kim, S. Kim, S. Y. Park, H. Kim and Y. S. Kim, Adv. Mater. 2013, 25, 2994.
20 D.-J. Yun and S.-W. Rhee, Thin Solid Films 2009, **517**, 4644.
21 P. Migliorato, M. Seok and J. Jang, Appl. Phys. Lett. 2012, **100**, 073506.
22 J.-H. Shin, J.-S. Lee, C.-S. Hwang, S.-H. Park, W.-S. Cheong, M. Ryu, C.-W. Byun, J.-I. Lee and H. Y. Chu, ETRI J. 2009, **31**, 62.